Binding and ordering of C_{60} on Pd(110): Investigations at the local and mesoscopic scale

J. Weckesser
Institut de Physique Expérimentale, Ecole Polytechnique Fédérale de Lausanne, PHB-Ecublens, CH-1015 Lausanne, Switzerland and Max-Planck-Institut für Festkörperforschung, Heisenbergstraße 1, D-70569 Stuttgart, Germany

C. Cepek
Physik Institut, Universität Zürich, Winterthurerstrasse 190, CH-8057 Zürich, Switzerland and Laboratorio Nazionale TASC-INFM, Padriciano 99, I-34012 Trieste, Italy

R. Fasel
Swiss Federal Laboratories for Materials Testing and Research (EMPA), CH-8600 Dübendorf, Switzerland

J. V. Barth[a)]
Institut de Physique Expérimentale, Ecole Polytechnique Fédérale de Lausanne, PHB-Ecublens, CH-1015 Lausanne, Switzerland

F. Baumberger and T. Greber
Physik Institut, Universität Zürich, Winterthurerstrasse 190, CH-8057 Zürich, Switzerland

K. Kern
Institut de Physique Expérimentale, Ecole Polytechnique Fédérale de Lausanne, PHB-Ecublens, CH-1015 Lausanne, Switzerland and Max-Planck-Institut für Festkörperforschung, Heisenbergstraße 1, D-70569 Stuttgart, Germany

(Received 18 June 2001; accepted 22 August 2001)

We present a comprehensive study on the binding and ordering of C_{60} on a Pd(110) surface employing scanning tunneling microscopy (STM), low-energy electron diffraction (LEED), x-ray photoelectron spectroscopy (XPS) and x-ray photoelectron diffraction (XPD). Three well-ordered structures evolving at elevated temperatures were identified, with $\begin{pmatrix} 7 & -1 \\ \mp 2 & \pm 5 \end{pmatrix}$, (4×5), (4×8) unit cells and a coverage of 1, 0.82 and 0.77 physical monolayers, respectively. The rearrangement of Pd substrate atoms turns out to play a crucial role in the evolution of thin C_{60} films. In STM images alternating bright and dark molecular rows are found for the regular structures. This height difference is attributed to a restructuring of the Pd substrate. Whereas the C_{60} molecules of the bright molecular rows are embedded in one layer deep microscopic pits, C_{60} accommodated in two layer deep pits account for the dark molecular rows. XPD results complete the understanding of the film structure. They reveal that the orientation of the C_{60} cages is unique in the regular structures; the molecules are facing with a 5–6 bond towards the substrate. © *2001 American Institute of Physics.* [DOI: 10.1063/1.1410391]

I. INTRODUCTION

The binding and ordering characteristics of fullerenes at solid surfaces have attracted much interest in recent years. In particular, the interaction of C_{60} with various metal surfaces was studied in detail[1–9] (for reviews, cf. Refs. 10, 11). On all investigated metals the fullerenes form a surface chemical bond, but the degree of hybridization of the C_{60} molecular orbitals with the substrate electronic states, and the amount of charge transfer differ significantly from substrate to substrate. At high coverages, generally close-packed overlayers evolve with a C_{60} intermolecular distance close to that of the van der Waals bonded C_{60} solid. Surprisingly, on some substrates different C_{60} species have been identified in scanning tunneling microscopy (STM) data.[9,12,13] The interpretation of this observation is not unique: both electronic effects reflecting different orientations of the C_{60} cages and a C_{60}-induced surface reconstruction have been invoked. For instance, on Ag(001) a dark and a bright C_{60} species can be distinguished in STM[13] and based on a x-ray photoelectron diffraction analysis Cepek *et al.* infer the coexistence of two C_{60} cage orientations.[14] However, the cage orientation seems not to be the origin for the contrast in STM that might rather be related to orientationally ordered and disordered C_{60} cages. On the other hand, strong substrate restructuring has been found for C_{60} on Ni(110)[3] and Au(110)[8]. For individual C_{60} molecules on Pd(110) a recent STM study revealed that C_{60} molecules reside on the (1×1) surface upon adsorption at intermediate temperatures and sink into the substrate resulting in a much higher C–Pd coordination upon thermal annealing.[15]

Here we present an investigation on the bonding and ordering of C_{60} on a Pd(110) surface using complementary experimental tools: STM, low-energy electron diffraction (LEED), x-ray photoelectron spectroscopy (XPS) and x-ray

a)Electronic mail: johannes.barth@epfl.ch

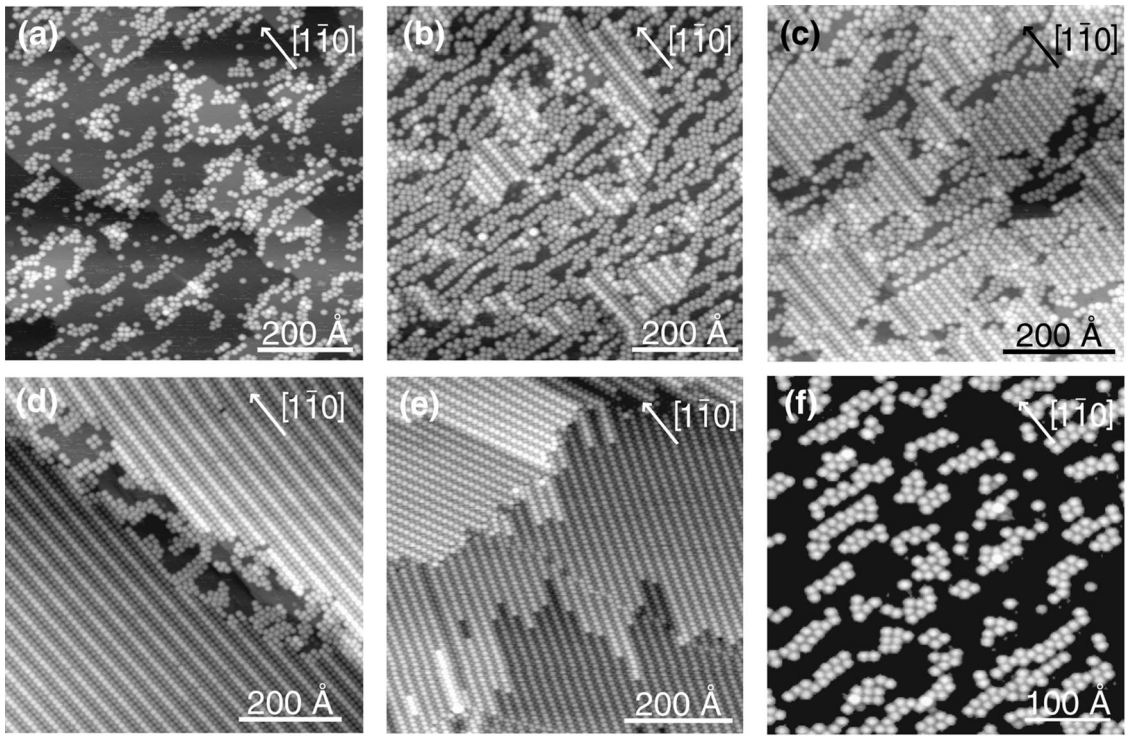

FIG. 1. Series of STM images demonstrating the coverage-dependent ordering of C_{60} on Pd(110) at elevated temperatures (700 K or as indicated). (a) At low coverage ($\Theta_{ph} \approx 0.2$) C_{60} stripes with a preferential width of two molecules form; Pd substrate atoms desorbing from the steps form Pd islands on the terraces in between C_{60} clusters. (b),(c) With increasing coverage a striped phase along the $[1\bar{1}0]$ substrate direction evolves which enlarges until nearly the entire surface is covered. Note that in the striped phase there are one or two dark rows between bright ones. (d) Well-ordered phase of alternating bright and two dark rows along $[1\bar{1}0]$ (annealed to about 970 K) which will be referred to as triple-stripe phase (in the center of the image there is an atomic step). (e) Saturated monolayer with alternating bright and dark molecular rows (annealed to about 920 K). Two domains rotated by about $\pm 22°$ with respect to $[1\bar{1}0]$ exist on the Pd(110) surface. (f) Upon annealing to 1050 K, the C_{60} molecules desorb without decomposition, whereby stripes with a preferential width of two molecules remain.

photoelectron diffraction (XPD). The evolution of the C_{60} films was followed in detail and three well-ordered structures evolving at elevated temperatures were identified by STM and LEED. The STM observations indicate furthermore that a substrate reconstruction is at the origin of bright and dark C_{60} rows observed in regular C_{60} films. XPD results reveal that the C_{60} molecules are generally oriented in the same way facing with a 5–6 bond towards the substrate.

II. EXPERIMENT

The experiments were performed in two different ultrahigh vacuum (UHV) setups. For STM a home-built variable temperature STM operational in the temperature range 40–800 K was employed. It is incorporated in a standard UHV chamber with a base pressure of $\approx 2 \times 10^{-10}$ mbar. The XPD and LEED experiments have been performed in a modified VG ESCALAB Mark II spectrometer[16] with a base pressure in the lower 10^{-11} mbar region. The same Pd(110) crystal was employed for all experiments. It was prepared by cycles of argon ion sputtering (700 eV, 4 μA/cm^2) and subsequent annealing (1000 K), resulting in large defect free terraces of typically 1000 Å width. C_{60} was deposited by a conventional Knudsen cell at background pressures of $\approx 5 \times 10^{-10}$ mbar. The employed deposition rate was $\approx 1 \times 10^{-5}$ ML/s as calibrated by STM and XPS (coverage given in terms of the saturated physical monolayer ($\Theta_{ph} = 1$ ML), where the ratio of adsorbed molecules per Pd surface atom is 0.12:1).

III. RESULTS AND DISCUSSION

First the evolution of the physical monolayer C_{60} on Pd(110) is addressed. C_{60} has been adsorbed on the Pd(110) surface held at room temperature followed by a high-temperature annealing cycle (700 K or as indicated). Evaporation of C_{60} on a Pd(110) surface held at the respective high temperature is equivalent. Elevated temperatures are necessary to produce well-ordered structures. In Fig. 1 a series of STM images illustrating the growth of C_{60} on Pd(110) is reproduced.

At low coverages [$\Theta_{ph} \approx 0.2$ in Fig. 1(a)]. C_{60} molecules are arranged in stripes with a preferential width of two molecules oriented roughly perpendicular to the close-packed Pd rows. On the flat terrace, Pd islands are found [same height of 1.4 Å as Pd(110) monatomic steps] which are edged by C_{60} clusters. This signals strong lateral C_{60}–Pd interactions, since Pd islands on flat terraces do not form in the absence of C_{60}. The Pd island formation reflects the presence of mobile Pd adatoms in the terraces at elevated temperatures. During the cooldown, the C_{60} molecules aggregate into clusters and simultaneously pin the metal adatoms. The imaging height of the C_{60} molecules (3.1 ± 0.2) Å is much lower than expected

from the hard-sphere diameter (7.1 Å). A similar value has been reported recently for isolated C_{60} molecules on Pd(110) annealed to high temperatures. STM imaging heights of adsorbed C_{60} falling significantly below the diameter of the carbon atom cage are a typical finding, and values in the range 2–6 Å have been reported for various systems (cf. Refs. 5, 17–19). With the present system, the value of the imaging height is moreover indicative of a substrate reconstruction, where C_{60} molecules drive the formation of microscopic pits, as revealed in a recent STM investigation.[15] These vacancies are two Pd layers deep and oriented along $[1\bar{1}0]$. In contrast, upon deposition at temperatures below 500 K, isolated C_{60} is bound on the Pd(110)(1×1) surface and typically appears as a 5.5 Å protrusion,[15] similar with the system C_{60}/Si(111)(7×7).[19] In the image reproduced in Fig. 1(b) almost the entire surface is covered with preferentially two molecule wide C_{60} stripes. They are oriented roughly perpendicular to the close-packed Pd rows, i.e., along the [001] direction. In view of the preferential adsorption of isolated C_{60} molecules in vacancies along $[1\bar{1}0]$, one might expect the formation of troughs in a missing row reconstruction, which would result in a linear ordering of C_{60} along $[1\bar{1}0]$. Apparently this is not the case and it is thus suggested that the surface reconstruction remains local as in the case of C_{60} on Au(110).[8] The islands' ordering is associated with indirect interactions mediated by elastic distortions of the substrate lattice (analogous to mesoscopic ordering phenomena driven by elastic distortions at other substrates, either pristine[20–22] or adsorbate-covered[23,24]). In addition to the stripes, patches of a well-ordered phase consisting of alternating dark and bright molecular rows oriented along $[1\bar{1}0]$ are discernable. Neighboring dark and bright rows are shifted by half a C_{60} molecular width resulting in a local quasihexagonal arrangement, whereas neighboring dark rows are in phase.

Upon increasing the coverage [Fig. 1(c)] the striped phase along $[1\bar{1}0]$ is covering nearly the entire surface. There are regions where dark and bright rows are alternating and others where there are *two* dark rows between bright ones. Upon annealing to about 970 K a well-ordered phase of alternating bright and two dark rows along $[1\bar{1}0]$ extends over the entire surface [cf. Fig. 1(d)] (in the center of the image there is an atomic step). The height difference between bright and dark rows is about (1.5 ± 0.2) Å, coming close to the substrate step height (1.38 Å). This single-domain structure, which will be referred to as triple-stripe phase, will be discussed below in more detail. Further increasing the coverage leads to another well-ordered phase extending over the entire surface [cf. Fig. 1(e)]. It consists of alternating dark and bright rows. The rows are rotated by about $\pm22°$ with respect to $[1\bar{1}0]$ and thus two domains exist. Since no additional molecules can be adsorbed in the first layer, this phase will be referred to as rotated-stripe phase as discussed following in more detail.

The data shown in Fig. 1 demonstrate in conjunction with the observed metastable C_{60} configuration reported earlier,[15] that altogether three topographically distinct C_{60} species can be found on a Pd(110) surface, which are characterized by a typical imaging height of (3.1 ± 0.2), (4.6 ± 0.2), and (5.5 ± 0.2) Å with respect to the substrate, respectively.

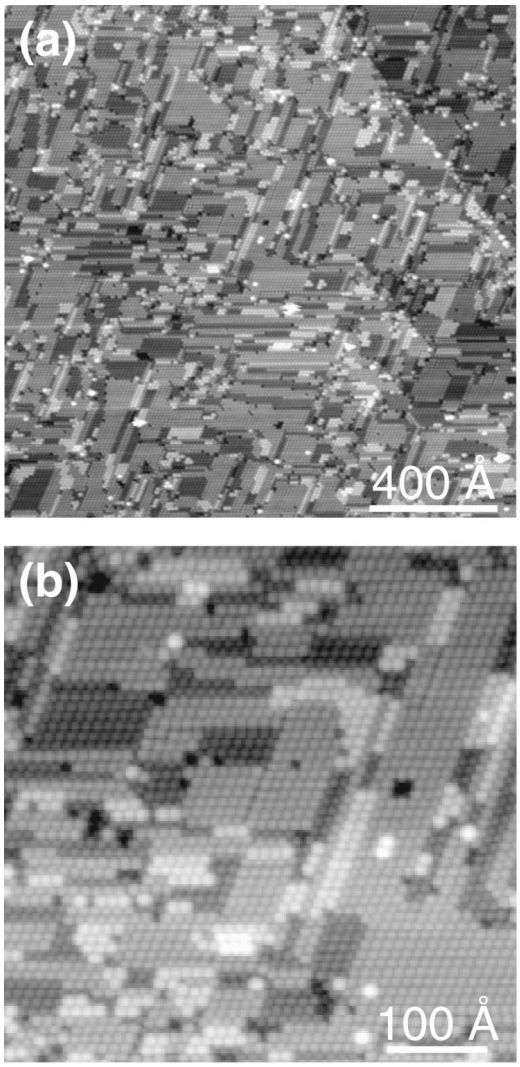

FIG. 2. (a) Surface roughening due to Pd mass transport in the presence of C_{60}. Upon annealing, a multilayer film too moderate to reach the equilibrium structure (720 K), a corrugated irregular metastable monolayer structure consisting of small C_{60} patches is formed. (b) Detail image of (a) showing the local quasihexagonal ordering of the C_{60} molecules. The height difference between neighboring patches corresponds to that of a monatomic substrate step.

In contrast to Pt(111) and Ni(110), where the C_{60} molecules have been found to decompose at 1050 K and 760 K respectively,[6,25] on Pd(110) C_{60} can be desorbed without decomposition at about 1050 K. Prior to complete desorption ($\approx$1100 K) clusters of a preferential width of two molecules remain, and finally, an almost clean Pd surface with some C_{60} molecules adsorbed at the upper step edges is obtained. This is remarkable as both palladium and nickel are group VIII *d*-metals in the same column of the periodic system with similar electronic structure (almost full *d*-band). On noble metal surfaces, e.g., Au(111), thermal desorption of C_{60} leaving a clean surface behind was reported and already occurs at temperatures of about 770 K.[26]

The low-coverage phase presented in Fig. 1(a) indicated that the mobility of substrate atoms interferes in the evolu-

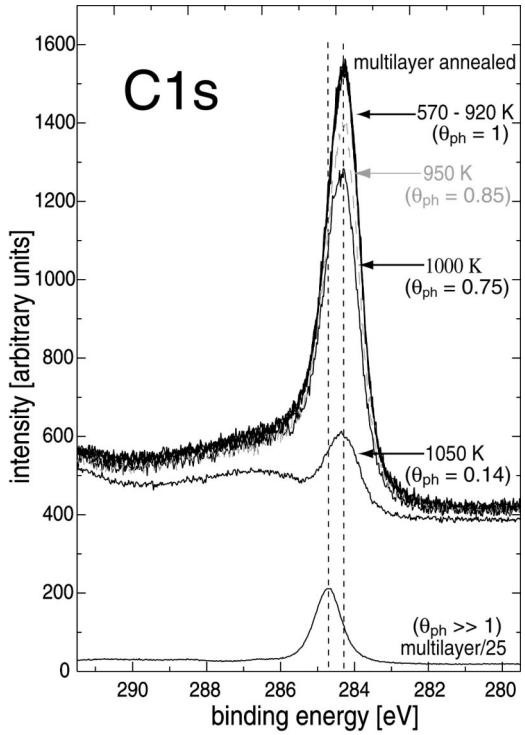

FIG. 3. XPS of the carbon 1*s* peak (using MgK_α radiation, $\hbar\omega = 1253.6$ eV) of a multilayer C_{60} film annealed to different temperatures normalized to photon flux (the multilayer peak is divided by 25 for comparison). The multilayer sublimates at 570 K; the saturated monolayer (defined as $\Theta_{ph}=1$) is stable up to about 920 K. Further annealing leads to stepwise losses at approximately 950 K ($\Theta_{ph}=0.85$) [measurement performed with a different pass energy, here a simulated spectrum (dashed gray) is included for illustration] and at 1000 K ($\Theta_{ph}=0.75$). At 1050 K most molecules are desorbed. The characteristic shift between multilayer and monolayer peak positions is indicated by the dashed lines.

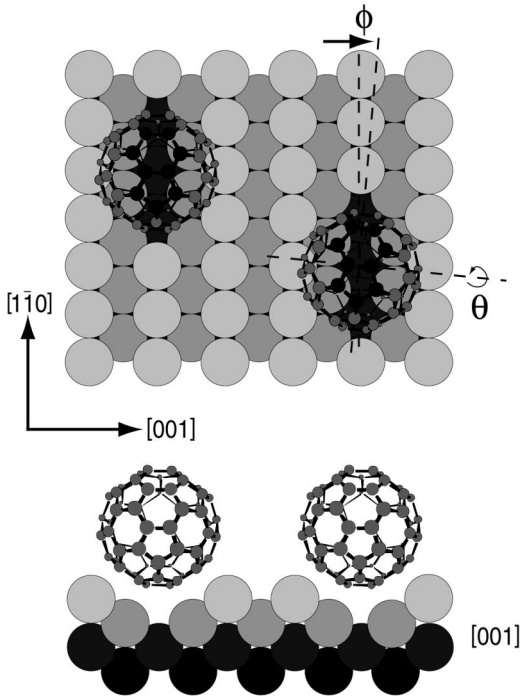

FIG. 4. Model of the typical 5–6 bonding configuration of C_{60} on a fcc(110) surface. The upper left C_{60} molecule is centered on a bond between a five- and a six-membered ring (drawn in black); the 5–6 bond is aligned along [001]. The lower right C_{60} molecule is rotated away from the high-symmetry bonding configuration by an azimuthal angle ϕ and a polar tilt θ. The situation upon thermal annealing is shown, where C_{60} induces a local reconstruction of the Pd(110) surface and is accommodated in microscopic pits (here taken one-layer deep). The corresponding increased C–Pd coordination is illustrated in the side view along [001].

tion of C_{60} films on Pd(110). This is corroborated by the STM topographs depicted in Fig. 2 showing a monolayer of C_{60} on Pd(110) which has been prepared by annealing a C_{60} multilayer film to 720 K. This temperature is insufficient to obtain long-range ordering and a metastable situation is encountered. In particular, it is obvious that two originally flat terraces have undergone a substantial roughening under the influence of the adsorbed molecules. Only upon further annealing to 920 K the well-ordered monolayer structure represented in Fig. 1(e) evolved in large regular domains. This observation provides clear evidence that substantial Pd atom rearrangements are involved in the formation of the well-ordered structures. In the detail image of Fig. 2(b) the local quasihexagonal ordering of the C_{60} molecules is revealed. The height difference between neighboring patches corresponds to a monatomic substrate step. Surface reconstruction going along with large substrate mass transport has similarly been observed for C_{60} adsorption on another *d*-metal, namely Ni(110).[3]

The most reliable way to follow the evolution of the different well-ordered structures of C_{60} on Pd(110) is multilayer deposition and subsequent annealing to increasingly higher temperatures (for the present experiments an annealing time of 60 seconds was chosen). In Fig. 3 the corresponding x-ray photoemission C1*s* peaks during such an experiment are depicted. The spectra have been taken with an MgK_α source ($\hbar\omega = 1253.6$ eV), an analyzer pass energy of 20 eV, corresponding to an overall energy resolution of ~0.8 eV, and are normalized to the same experimental conditions and incident photon flux. For comparison the multilayer peak is divided by a factor of 25. At about 455 K multilayer desorption sets in.[27] Spectra taken following annealing to temperatures in the range 570–920 K are identical and associated with a saturated monolayer. Further annealing to ≈950 and ≈1000 K leads to stepwise losses of C_{60} bound in the monolayer film. Finally, upon reaching a temperature of ≈1050 K, only a small amount of carbon remains on the surface.

The multilayer C1*s* peak is centered at $E_{kin}=969.8$ eV with a FWHM of 0.8 eV, whereas the monolayer peaks are shifted by 0.4 eV to 970.2 eV with a FWHM of 1.1 eV and an asymmetric line shape towards higher binding energies. Similar results have been reported, e.g., for C_{60} on Au(110), Ag(111)[9] and on Pt(111)[7]. One origin for the different C1*s* peak positions might be the C_{60} charge state, since for a negatively charged molecule the photoemission line shows a chemical shift towards lower binding energies.[7] On the other hand a so-called relaxation shift, reflecting the metal-substrate screening of the core hole created in the photoabsorption process, is typical for molecules interacting with metal surfaces.[28] For *n*-hexatriacontane, a saturated hydrocarbon, adsorbed on Cu(111) the shift of 0.8 eV is much

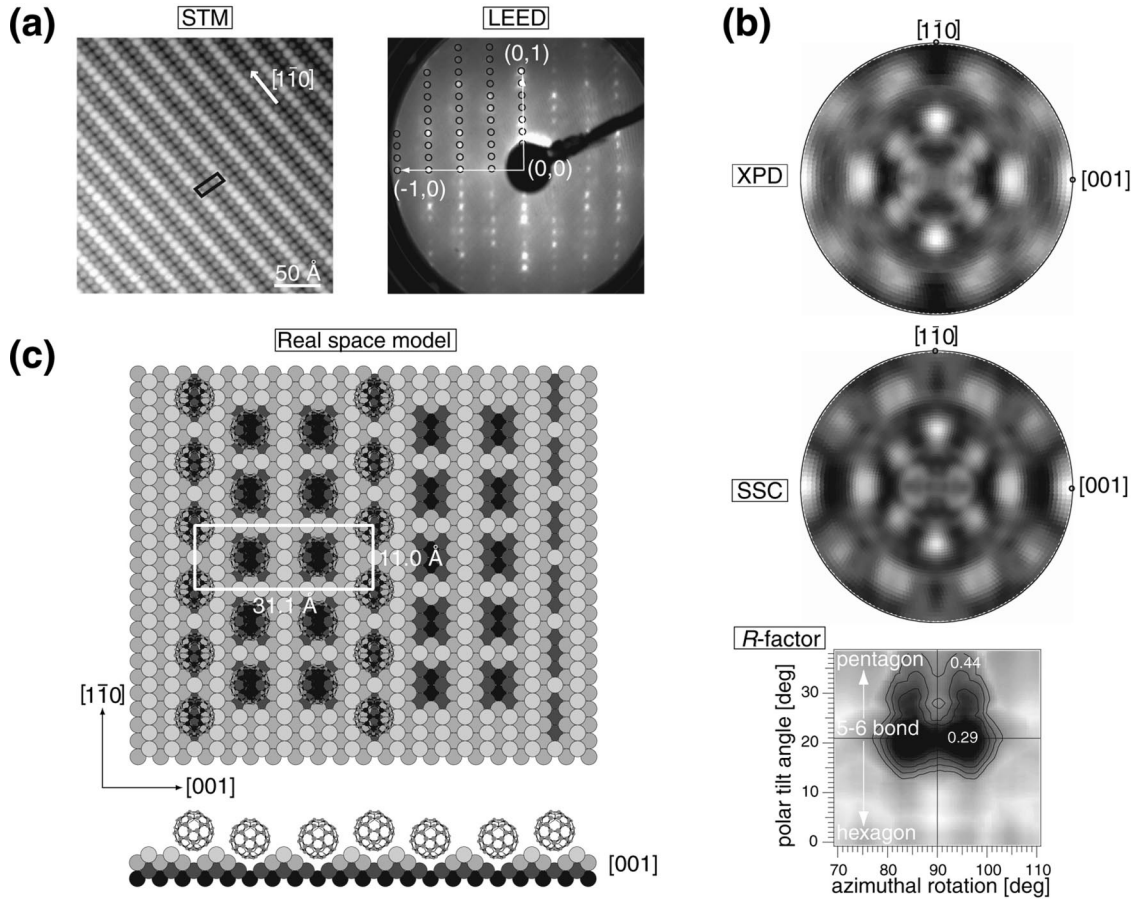

FIG. 5. (a) STM image of the triple-stripe phase (multilayer C_{60} annealed to 1000 K) consisting of alternating bright and two dark rows oriented along $[1\bar{1}0]$. In the corresponding LEED pattern ($E=38.1$ eV) the simulated spots for a (4×8) structure are overlaid. (b) Experimental C1*s* XPD pattern ($E_{kin}=970$ eV) and SSC calculation for the optimized molecular orientation which fits the experimental data. The *R*-factor plot obtained by azimuthal rotation and polar tilt of the C_{60} molecules away from the symmetric 5–6 orientation, as schematically shown in Fig. 4, yields a molecular orientation of $\Delta\phi=\pm(5\pm2)°$ (the symmetric 5–6 bond corresponds to $\theta=20.9°$ and $\phi=90°$). (c) Suggested real-space model: The bright molecular rows seen in STM correspond to C_{60} molecules adsorbed in a vacancy formed by Pd atoms released out of the first layer. The dark molecular rows correspond to C_{60} molecules adsorbed in a vacancy formed by Pd atoms released out of the first *two* layers. On the right side the C_{60} molecules are omitted to illustrate these vacancies. In the side view along [001] the alternating dark and bright rows are clearly discernible. The unit cell contains three C_{60} molecules, the area per C_{60} molecule amounts to 77.3 $Å^2$ fitting well to the measured C1*s* intensity of 75% with respect to rotated-stripe phase (saturated monolayer).

larger, but in this case all C atoms are in the proximity of the substrate.[29] The broadening of the C_{60} monolayer peaks is thus associated with nonequivalent carbon sites on the molecule and/or creation of electron-hole pairs. For a detailed analysis of C_{60} C1*s* peak positions and line shapes see Ref. 7. Defining the coverage of the film annealed to 570–920 K as 100% (saturated monolayer), the coverage of the films annealed to 950 K and 1000 K can be determined from the integrated peak intensities to be 85% and 75%, respectively. Upon annealing to 1050 K the remaining coverage amounts to 14%.

In the following we will focus on the well-ordered structures. In addition to STM observations, LEED and XPD measurements have been performed to characterize the binding and ordering on the local and mesoscopic scale. The molecular shape of C_{60} consists of 5- and 6-membered rings, and in recent work, it has been suggested that the internal molecular structure in STM images can be used to determine the molecular orientation of adsorbed C_{60}.[19,30–32] But this is a quite delicate procedure, strongly dependent on the nature of the STM tip and requiring elaborate model calculations. We have determined the molecular orientation of the adsorbed C_{60} with high precision by x-ray photoelectron diffraction. XPD patterns are a real-space ''fingerprint'' of the molecular orientation, by symmetry arguments alone, restrictions of the possible molecular orientations can immediately be made. Guidice *et al.* speculated that different molecular orientations are responsible for dark and bright rows seen in the STM images of C_{60} on Ag(001).[13] With the present system the rotated-stripe phase consists of alternating dark and bright rows, whereas in the triple-stripe phase *two* dark rows exist in between bright rows. The different ratios of these two species of 2:1 in the triple-stripe and 1:1 in the rotated-stripe phase of C_{60} on Pd(110) allows one to directly check this hypothesis with the present system. As the XPD patterns are related in a straightforward way to the orientation of the C_{60} molecules, it immediately follows that they should be different for the two well-ordered phases if the molecules within dark and bright rows were oriented differently. A variety of C_{60} cage orientations have been observed by XPD for the different single crystal metal surfaces studied so far. On Cu(111) and Al(111), C_{60} is adsorbed on a six-membered

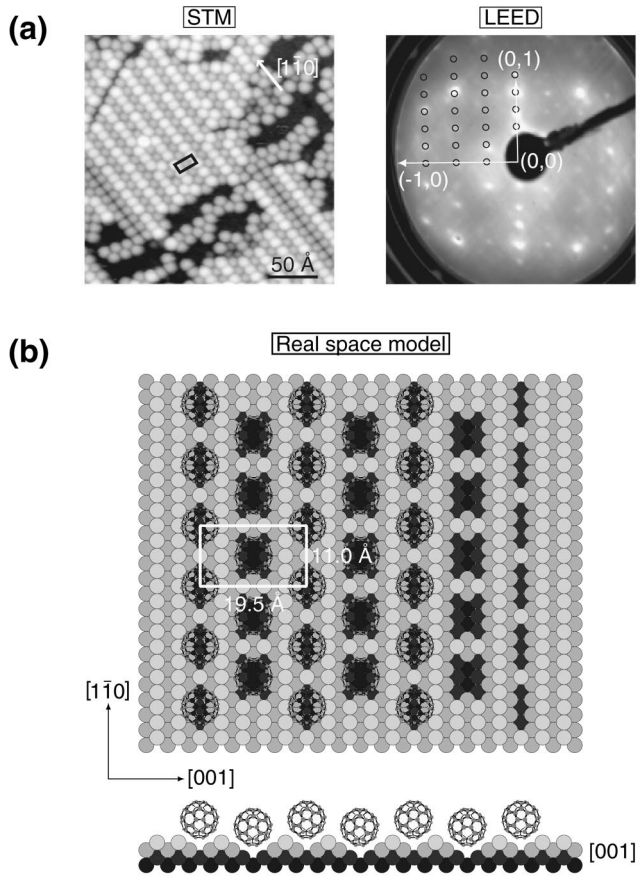

FIG. 6. (a) STM image showing domains of alternating bright and dark rows along $[1\bar{1}0]$ prepared by submonolayer C_{60} deposition at 720 K. This structure covers the entire surface when a C_{60} multilayer film is annealed to $T=950$ K. In the corresponding LEED pattern ($E=38.1$ eV) the simulated (4×5)-spots are overlaid. (b) Real-space model: Dark and bright C_{60} rows can be similarly explained as in the triple-stripe phase [for a detailed description see the caption of Fig. 5(c)]. The unit cell contains two C_{60} molecules, the area per C_{60} molecule amounts to 107.0 $Å^2$ fitting well to the measured C1*s* intensity of 85% with respect to the rotated-stripe phase (saturated monolayer).

ring, on Al(001) on a C edge atom. On fcc surfaces such as Cu(110) and Ni(110)[33] a 5–6 bond orientation was reported.[1,4] This configuration is illustrated in Fig. 4: the molecule faces to the substrate with a five- and a six-membered ring (drawn in black) of the C_{60} cage. The 5–6 bond was found to be aligned along the [001]-direction of the fcc(110) surfaces.[1,4] We show the situation for C_{60} molecules inducing a hypothetic local surface reconstruction on Pd(110), where C_{60} are accommodated in one-layer deep microscopic pits (for the isolated stabilized species two-layer deep pits were concluded[15]). The corresponding increased C–Pd coordination can be seen in the side view along [001]. The C_{60} molecule shown in the lower right of the model is slightly rotated away from the high symmetric 5–6 bonding configuration by an azimuthal angle ϕ and a polar tilt θ.

Figure 5(a) shows an STM image and the corresponding LEED pattern of the triple-stripe phase evolving upon annealing a C_{60} multilayer on Pd(110) to 1000 K. The coverage determined by means of XPS amounts to 75% relative to the saturated monolayer. In STM this structure consists of *two* dark rows in between bright ones running along $[1\bar{1}0]$, resulting in a single domain on the Pd(110) surface. Neighboring dark and bright rows are shifted by half a molecular width and snap in, whereas neighboring dark rows are in phase. The height difference between dark and bright rows is (1.5 ± 0.2) Å which is approximately the height of a monatomic step on the Pd(110) surface (1.38 Å). This height variation is independent of the tunneling parameters and is thus interpreted as topographic difference. The LEED pattern is easily determined to be a rectangular (4×8) structure (simulated spots are overlaid), confirming that the C_{60} rows are aligned parallel to the close-packed Pd rows along $[1\bar{1}0]$.

The corresponding XPD measurements are represented in Fig. 5(b). The anisotropy of the pattern taken at room temperature reflects a high orientational order of the C_{60} cages and rules out the possibility of freely rotating ''buckyballs.'' Single-scattering cluster (SSC) calculations performed for different high-symmetry orientations on a twofold substrate[34] reveal that the XPD pattern is typical for a 5–6 bonding configuration (cf. Fig. 4). In order to exactly determine the molecular orientation, we have performed an extensive *R*-factor analysis comparing the experimental C1*s* diffraction pattern to SSC calculations, allowing the C_{60} molecules to rotate away from the ideal 5–6 orientation. The SSC calculations for the optimized molecular orientation and the resulting *R*-factor plot are shown as well in Fig. 5(b). The SSC calculations nicely reproduce the experimental data. As can be seen from the *R*-factor plot obtained by azimuthal rotation $\Delta\phi$ and polar tilt $\Delta\theta$ of the C_{60} molecules away from the symmetric 5–6 orientation (corresponding to $\theta=20.9°$ and $\phi=90°$), the best agreement is achieved at $\Delta\phi=\pm(5\pm2)°$. An identical azimuthal rotation is reported for C_{60} adsorbed on Cu(110).[4] The polar tilt $\Delta\theta$ is basically 0° for the present case, whereas on Cu(110) the C_{60} molecules are tilted by $\Delta\theta=+4.5°$ (inclined towards the bottommost pentagon). The XPD results show that there is a unique C_{60} cage orientation.

As already pointed out in the description of the growth scenario, the rearrangement of Pd substrate atoms plays a crucial role in the film evolution. Furthermore, for isolated C_{60} molecules on Pd(110), a thermally activated bonding transition has been reported (upon annealing to $\approx$700 K the C_{60} molecules accommodate in microscopic pits resulting in a higher C–Pd coordination[15]). It is hence concluded that the different heights of bright and dark rows are due to a surface reconstruction.

With the real space model presented in Fig. 5(c), which is based on geometrical reasoning, all aspects of STM, LEED and XPD data are rationalized. Whereas the bright molecular rows are composed of C_{60} molecules adsorbed in a vacancy formed by released Pd atoms of the first layer, the dark molecular rows consist of C_{60} molecules adsorbed in a vacancy formed by Pd atoms released out of the first *two* layers. On the right side the C_{60} molecules are omitted to illustrate the different vacancies. By analogy to the low-coverage situation on Pd(110) [cf. Fig. 1(b) and Ref. 15] and the structure reported for the C_{60}/Au(110) system,[8] the reconstruction is assumed to remain local and thus isolated vacancies are used in the real space model and no extended

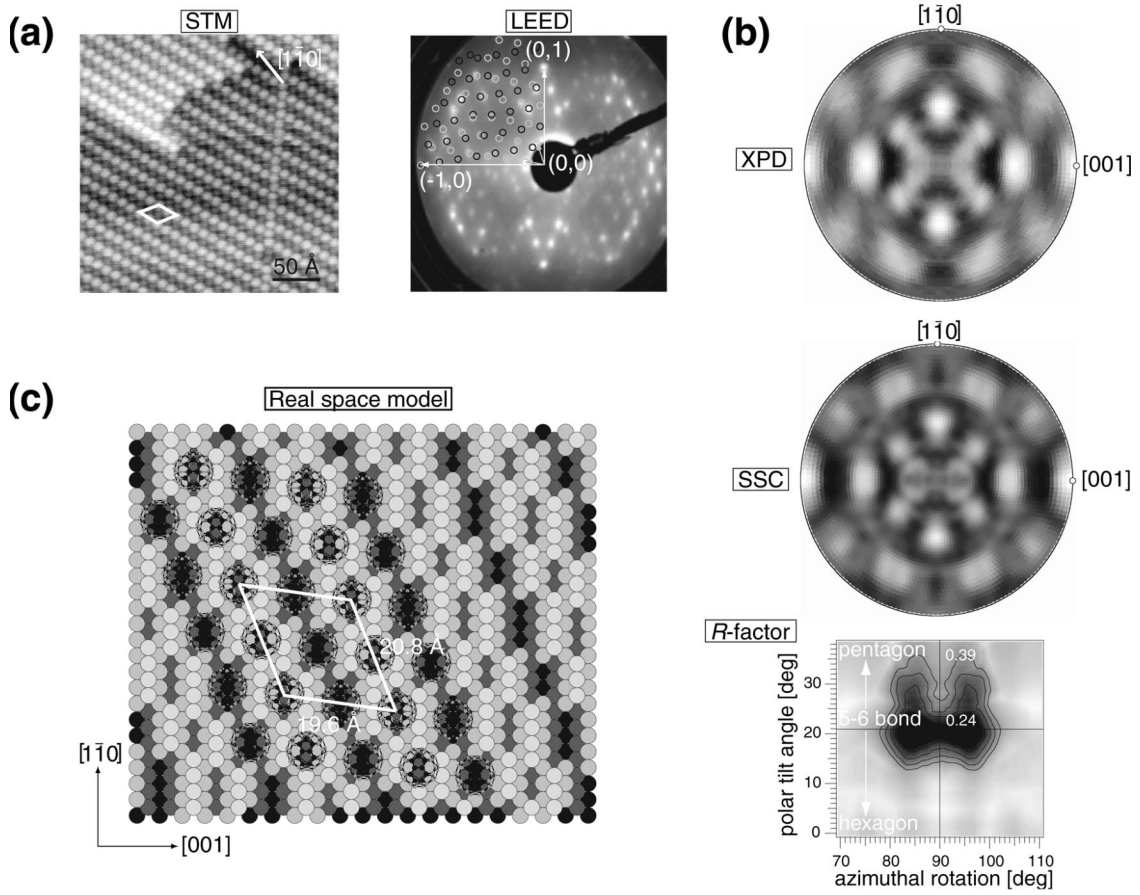

FIG. 7. (a) STM image of the rotated-stripe phase. Alternating bright and dark rows are rotated by about 22° with respect to $[1\bar{1}0]$ and shifted by half a molecular width. In the corresponding LEED pattern ($E=38.1$ eV) the simulated spots of the $(\frac{7}{\mp 2}\ \frac{1}{\pm 5})$ structure [2 domains, cf. Fig. 1(e)] are overlaid. (b) Experimental C1*s* XPD pattern ($E_{kin}=970$ eV) and SSC calculation for the optimized molecular orientation which fits the experimental data. The *R*-factor plot obtained by azimuthal rotation and polar tilt of the C_{60} molecules away from the symmetric 5–6 orientation, as schematically shown in Fig. 4 yields a molecular orientation of $\Delta\phi=\pm(5\pm2)°$ (the symmetric 5–6 bond corresponds to $\theta=20.9°$ and $\phi=90°$). The XPD data are comparable to the ones for the triple-stripe phase represented in Fig. 5(b). (c) Real-space model: Dark and bright C_{60} rows can be similarly explained as in the (4×5) and (4×8) structure. For a detailed description see the caption of Fig. 5(c). The unit cell contains four C_{60} molecules, the area per C_{60} molecule amounts to 88.2 Å^2.

troughs along $[1\bar{1}0]$. Note that in contrast to the x-ray diffraction analysis performed for the C_{60}/Au(110) system, the detailed atomic arrangement of the reconstructed substrate cannot be conclusively unraveled on the basis of the present results. However, the chemical reactivity of the C_{60}-facets and the preference of a distinct bonding configuration for the adsorbed C_{60} molecules indicate that local pits are formed as with the Au(110) substrate.

The alternating dark and bright rows are clearly discernible in the side view along [001] [cf. Fig. 5(c)]. The geometric height difference between the rows corresponding to a monatomic step (1.38 Å) is in agreement with the observed height difference of (1.5 ± 0.2) Å in STM images. The C_{60} molecules in the dark rows are assumed to be identically bound as the stable C_{60} species at low coverages (cf. Ref. 15) explaining the similar observed height of (3.1 ± 0.2) Å. This geometry allows for strong bonding due to high C–Pd coordination. The C_{60} molecular height in the bright rows is (4.6 ± 0.2) Å, i.e., just in between the one of the stable and that of the metastable C_{60} species found at low coverage.[15] This can be rationalized with the proposed model: C_{60} molecules in the dark rows are adsorbed in a two-layer deep vacancy (as the stable C_{60} species), C_{60} molecules in the bright rows in a one-layer deep vacancy, and the metastable C_{60} species on top of the unreconstructed Pd(110) surface. The C_{60} molecules are facing with a 5–6 bond to the surface which is rotated by $\Delta\phi=\pm(5\pm2)°$ away from the [001] direction as determined by XPD. The bright C_{60} molecules are centered in a local quasihexagonal structure with an intermolecular distance of 11.0 Å along $[1\bar{1}0]$ (10% expansion with respect to the close-packed plane in a C_{60} crystal) and 11.3 Å along $[4\bar{4}5]$ and $[\bar{4}45]$ (12% expansion) (taking the STM height difference of 1.5 Å into account); the distance between neighboring dark rows amounts to 11.7 Å. The area of the unit cell containing three C_{60} molecules amounts to 342.3 Å^2 giving 114.1 Å^2 per molecule, which fits well to the XPS-derived density.

These observations are in line with the significant interfacial restructuring upon C_{60} adsorption on Ni(110) via the addition/removal of Ni [001] rows reported by Murray *et al.*[3] The corresponding increase of the C_{60} coordination to the substrate was associated with the energetic proximity of the C_{60} LUMO and metal *d*-states leading to strong hybridiza-

TABLE I. Main characteristics of the regular phases formed in the C_{60}/Pd(110) system.

Phase	Unit cell	$T_{annealing}$ [K]	Coverage [Θ_{ph}]	Area per C_{60} [Å^2]	Cage orientation
Rotated-stripe	$\begin{pmatrix} 7 & -1 \\ \mp 2 & \pm 5 \end{pmatrix}$	920	1	88.2	5–6 bond $\Delta\phi = \pm(5\pm 2)°$, $\Delta\theta = (0\pm 1)°$
(4×5)	(4×5)	950	0.82	107.0	⋯
Triple-stripe	(4×8)	1000	0.77	114.1	5–6 bond $\Delta\phi = \pm(5\pm 2)°$, $\Delta\theta = (0\pm 1)°$

tion. In view of the related electronic structures of nickel and palladium, especially the almost full *d*-band, and the comparable work functions of 5.04 eV and 5.13 eV,[35] a similar argumentation can be invoked for the Pd(110) surface.

The well-ordered structures were prepared by slowly heating a C_{60} multilayer on Pd(110) in front of the LEED optics until a clear pattern could be observed. At about $T = 950$ K a second structure showing sharp LEED spots evolves [cf. Fig. 6(a)]. The LEED pattern is easily determined to be a (4×5) structure (simulated spots are overlaid). This structure is associated with the C_{60} arrangement shown in the STM image aside, where a structure consisting of alternating dark and bright rows along $[1\bar{1}0]$ on small areas is reproduced [cf. Fig. 1(c)]. As in the case of the triple-stripe phase, the rows are aligned along the close-packed Pd rows and thus only one domain exists on the Pd(110) surface. In Fig. 6(b) a real-space model compatible with STM and LEED observations is presented. Similar to the triple-stripe phase the accommodation of the molecules in microscopic pits explains the observed height difference in STM in a natural way. The C_{60} molecules are centered in a local quasihexagonal structure with the same intermolecular distances as in the triple-stripe phase. Two C_{60} molecules are in the 214.0 Å^2 large unit cell giving 107.0 Å^2 per molecule. An XPD analysis of this phase was not performed.

Upon annealing a C_{60} multilayer to 920 K, the physical monolayer remains saturated and the rotated-stripe phase is formed. In the corresponding STM data, alternating dark and bright rows which are rotated by about $\pm 22.0°$ with respect to the $[1\bar{1}0]$ surface direction are resolved [cf. Figs. 1(e) and 7(a)]. Locally, the C_{60} molecules form a close-packed quasihexagonal arrangement. Due to the twofold symmetry of the Pd(110) surface, two superstructure domains exist. Neighboring rows are shifted by half a molecular width and snap in. The height difference between dark and bright rows is (1.3 ± 0.2) Å, which is about the height of a monatomic step on the Pd(110) surface (1.38 Å). The corresponding LEED pattern reflects the two domains visible in STM data [cf. Fig. 1(e)]. The corresponding unit cell is determined to $\left(\begin{smallmatrix} 7 & -1 \\ \mp 2 & \pm 5 \end{smallmatrix}\right)$, where ± 5 and ∓ 2 accounts for the two possible domain orientations. The simulated spots for this structure are overlaid in the LEED pattern; spots from the two domains are indicated in black and gray, respectively. The corresponding XPD measurements are represented in Fig. 7(b). Despite the different stripe orientations and the different ratios of dark and bright rows in the rotated-stripe and the triple-stripe phase, their XPD patterns are comparable [cf. Figs. 5(b) and 7(b)], unambiguously demonstrating that the orientation of the C_{60} cages in the dark and bright rows is identical. Consequently the real-space model represented in Fig. 7(c) for the rotated-stripe phase is proposed. The angle between the C_{60} rows and $[1\bar{1}0]$ is 22.0°, and the corresponding angle of 44° between the domains fits well with the measured value of ≈45° in the STM data. The molecular stripes of the phase can be explained with an analogue surface reconstruction as for the (4×8)- and (4×5)-phases. Note however, that within a molecular row both fourfold hollow and long-bridge sites (shifted by half a lattice constant in $[1\bar{1}0]$) have to be assumed in the rotated-stripe phase, whereas in the (4×8)- and (4×5)-structure, all sites are identical. The height difference between the two different adsorption sites is ≈0.2 Å in a hard-sphere model, which is small compared to the height difference of (1.3 ± 0.2) Å between dark and bright molecular rows. Pedersen *et al.* report of C_{60} on Cu(110).[2] They find a height difference of about 0.1 Å between adsorption in fourfold hollow and long-bridge sites only in high-resolution STM images. In our STM data this feature was not observed. In the rotated-stripe phase C_{60} forms a close-packed quasihexagonal overlayer that is expanded by 1% with respect to the bulk C_{60} close-packed plane. The intermolecular distances are 10.38 Å along $[7\bar{7}2]$ (3% expansion), 9.89 Å along $[\bar{1}15]$ (1% compression) and 10.17 Å along $[22\bar{1}]$ (1% expansion) (taking the STM height difference of 1.3 Å into account). Similar behavior has been reported for C_{60} adsorption on other single crystal metal surfaces.[30,31,36,37] Subtle variations in the hexagonal overlayer structure have often been observed, but the bulk C_{60} NN distance is, in most cases, closely retained. For C_{60} on Cu(110) the intermolecular distances vary from 9.6 Å to 11.1 Å, depending on which neighboring pairs are considered.[3,4] The 353.0 Å^2 large unit cell in the rotated-stripe phase contains four C_{60} molecules, giving 88.2 Å^2 per molecule. This yields a calculated coverage of 77% and 82% for the (4×8) and (4×5) structures [cf. Figs. 5(c) and 6(b)] respectively, in good agreement with the values of 75% and 85% determined by means of XPS.

Finally, we address the cage orientation in C_{60} films formed at room temperature. In this case a metastable bonding configuration was observed by STM, where the molecules are residing on the Pd(110)(1×1) surface.[15] A corresponding XPD/SSC analysis performed for a coverage of $\Theta_{ph}\sim 0.4$ reveals that again the 5–6 bonding prevails. However, subtle differences with respect to the well-ordered lay-

ers exist. While the azimuthal rotation of the 5–6 bonds away from the [001] direction is again $\Delta\phi = \pm(5\pm2)°$, the polar tilt angle amounts now to $\Delta\theta = -(5\pm1)°$. This significant tilting, which is in contrast to the cage orientation in the regular phases, is associated with the missing lateral C_{60}–Pd coordination. Interestingly, the tilt for 5–6 bonded C_{60} on a Cu(110) surface has an opposite orientation ($\Delta\theta = +(4.5\pm1)°$), while the azimuthal rotation is again $\Delta\phi = \pm(5\pm2)°$.[4] Hence it seems that on the fcc(110) transition metal surfaces investigated so far the substrate symmetry accounts for the preference of the 5–6 bond with a certain azimuth, while the tilting of the C_{60} cage is adjusted according to the substrate's chemical nature and the local bonding environment. It will be interesting to see whether this is a general trend.

IV. SUMMARY

The binding and ordering of C_{60} on a Pd(110) surface has been studied by the complementary use of multiple experimental techniques. Distinct well-ordered striped phases could be identified upon annealing C_{60} films to elevated temperatures, as summarized in Table I. The results reveal in particular that with all regular phases a reconstruction of the substrate is encountered, whereby the same orientation of the C_{60} cage with respect to the surface occurs, i.e., 5–6 bonds are formed.

[1] R. Fasel, P. Aebi, R. G. Agostino, D. Naumovic, J. Osterwalder, A. Santaniello, and L. Schlapbach, Phys. Rev. Lett. **76**, 4733 (1996).
[2] M. Ø. Pedersen, P. W. Murray, E. Laegsgaard, I. Stensgaard, and F. Besenbacher, Surf. Sci. **389**, 300 (1997).
[3] P. W. Murray, M. Ø. Pedersen, E. Laegsgaard, I. Stensgaard, and F. Besenbacher, Phys. Rev. B **55**, 9360 (1997).
[4] R. Fasel, R. G. Agostino, P. Aebi, and L. Schlapbach, Phys. Rev. B **60**, 4517 (1999).
[5] M. T. Cuberes, R. R. Schlittler, and J. K. Gimzewski, Appl. Phys. A: Mater. Sci. Process. **66**, 669 (1998).
[6] C. Cepek, A. Goldoni, and S. Modesti, Phys. Rev. B **53**, 7466 (1996).
[7] M. Pedio, K. Hevesi, N. Zema, M. Capozi, P. Perfetti, R. Gouttebaron, J. J. Pireaux, R. Caudano, and P. Rudolf, Surf. Sci. **437**, 249 (1999).
[8] M. Pedio, R. Felici, X. Torrelles, P. Rudolf, M. Capozi, J. Rius, and S. Ferrer, Phys. Rev. Lett. **85**, 1040 (2000).
[9] J. K. Gimzewski, S. Modesti, and R. R. Schlittler, Phys. Rev. Lett. **72**, 1036 (1994).
[10] P. Rudolf, in *Proceedings of the International Winterschool on Electronic Properties of Novel Materials. Fullerenes and Fullerene Nanostructures* (World Scientific, Singapore, 1996), pp. 263.
[11] A. V. Hamza, in *Fullerenes: Chemistry, Physics and Technology*, edited by K. M. Kadish and R. S. Ruoff (Wiley, New York, 2000), p. 531.
[12] X. Yao, R. K. Workman, C. A. Peterson, D. Chen, and D. Sarid, Appl. Phys. A: Mater. Sci. Process. **66**, 107 (1998).
[13] E. Giudice, E. Magnano, S. Rusponi, C. Boragno, and U. Valbusa, Surf. Sci. **405**, L561 (1998).
[14] C. Cepek, R. Fasel, M. Sancrotti, T. Greber, and J. Osterwalder, Phys. Rev. B **63**, 125406 (2001).
[15] J. Weckesser, J. V. Barth, and K. Kern, Phys. Rev. B **64**, 161403 (2001).
[16] J. Osterwalder, P. Aebi, R. Fasel, D. Naumovic, P. Schwaller, T. Kreutz, L. Schlapbach, T. Abukawa, and S. Kono, Surf. Sci. **331–333**, 1002 (1995).
[17] Y. Z. Li, M. Chander, J. C. Patrin, J. H. Weaver, L. P. F. Chivante, and R. E. Smalley, Phys. Rev. B **45**, 13837 (1992).
[18] C. Chavy, C. Joachim, and A. Altibelli, Chem. Phys. Lett. **214**, 569 (1993).
[19] J. I. Pascual, J. Gómez-Herrero, C. Rogero, A. M. Baró, D. Sánchez-Portal, A. Artacho, P. Ordejón, and J. M. Soler, Chem. Phys. Lett. **321**, 78 (2000).
[20] V. I. Marchenko, JETP Lett. **33**, 381 (1981).
[21] J. V. Barth, H. Brune, R. J. Behm, and G. Ertl, Phys. Rev. B **42**, 9307 (1990).
[22] S. Narasimhan and D. Vanderbilt, Phys. Rev. Lett. **69**, 1564 (1992).
[23] K. Kern, H. Niehus, A. Schatz, P. Zeppenfeld, J. George, and G. Comsa, Phys. Rev. Lett. **67**, 855 (1991).
[24] D. Vanderbilt, Surf. Sci. **268**, L300 (1992).
[25] M. R. C. Hunt, S. Modesti, P. Rudolf, and R. E. Palmer, Phys. Rev. B **51**, 10039 (1995).
[26] E. I. Altman and R. J. Colton, Surf. Sci. **279**, 49 (1992).
[27] L. H. Tjeng, R. Hesper, A. C. L. Heessels, A. Heeres, H. T. Jonkman, and G. A. Sawatzky, Solid State Commun. **103**, 31 (1997).
[28] G. Witte and C. Wöll, J. Chem. Phys. **103**, 5860 (1995).
[29] K. Weiss, J. Weckesser, and C. Wöll, J. Mol. Struct.: THEOCHEM **458**, 143 (1999).
[30] E. I. Altman and R. J. Colton, Phys. Rev. B **48**, 18244 (1993).
[31] T. Hashizume, K. Motai, X. D. Wang *et al.*, Phys. Rev. Lett. **71**, 2959 (1993).
[32] J. G. Hou, Y. Jinlong, W. Haiqian *et al.*, Phys. Rev. Lett. **83**, 3001 (1999).
[33] R. Fasel (unpublished).
[34] R. Fasel, Ph.D. thesis, Université de Fribourg (Switzerland 1996).
[35] K. Yagi, K. Higashiyama, S. Yamazaki, H. Yanashima, H. Ohnuki, H. Fukutani, and H. Kato, Surf. Sci. **231**, 397 (1990).
[36] Y. Kuk, D. K. Kim, Y. D. Suh, K. H. Park, H. P. Noh, S. J. Oh, and S. K. Kim, Phys. Rev. Lett. **70**, 1948 (1993).
[37] J. K. Gimzewski, S. Modesti, C. Gerber, and R. R. Schlittler, Chem. Phys. Lett. **213**, 401 (1993).